Chemosphere 216 (2019) 31–39

Contents lists available at ScienceDirect

Chemosphere

journal homepage: www.elsevier.com/locate/chemosphere

Sedimentary record of polycyclic aromatic hydrocarbons in mud deposits along the southeastern coast of Liaodong Peninsula and its relation to the anthropogenic and natural activities in the Northeast China

Chenglong Wang [a, b], Qiang Liu [a, b], Jianhua Gao [a, b, *], Hui Sheng [a, b], Qiao Ai [a, b], Yong Shi [a, b], Daolai Zhang [c], Yaping Wang [a, b]

[a] Key Laboratory of Coast and Island Development (Nanjing University), Ministry of Education, Nanjing 210093, China
[b] School of Geographic and Oceanographic Sciences, Nanjing University, Nanjing 210093, China
[c] Qingdao Institute of Marine Geology, Qingdao 266071, China

HIGHLIGHTS

- We explored historical PAH records in coastal mud deposits of the North Yellow Sea.
- Sedimentary records of PAHs reflect trends in socio-economic development.
- Sedimentary PAH records can reflect historical transformations in energy sources.
- Sedimentary records of PAHs can also reflect the fire events over a regional scale.

GRAPHICAL ABSTRACT

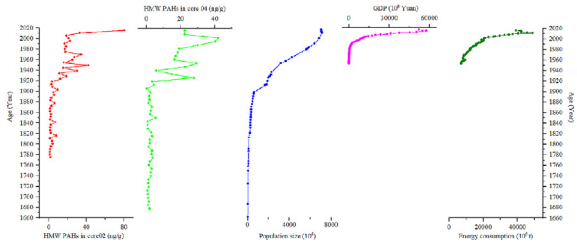

ARTICLE INFO

Article history:
Received 28 June 2018
Received in revised form
28 August 2018
Accepted 15 October 2018
Available online 19 October 2018

Handling Editor: Patryk Oleszczuk

Keywords:
Polycyclic aromatic hydrocarbons
Sedimentary record
Population migration
Energy consumption
Fire events
Northeast China

ABSTRACT

The concentrations of polycyclic aromatic hydrocarbons (PAHs) in two ^{210}Pb-dated sediment cores collected from mud deposits along the southeastern coast of the Liaodong Peninsula were investigated to reconstruct the sedimentary records of PAHs and their relationship with anthropogenic and natural activities. The concentrations of 16 PAHs (∑PAHs) were low and remained stable before the year 1820, reflecting an autarkic agricultural civilization. From 1820 to 1900, with the gradual lifting of prohibition, people migrated into Northeast China, resulting in the release of large amounts of ∑PAHs into the environment. At the beginning of the 1900s, the ∑PAH levels in the two cores displayed increasing trends with significant fluctuations, linked to a period of social turbulence with continuous wars in Northeast China. After 1949, vertical ∑PAH trends in the cores predominantly reflected trends in economic development. Based on the different PAH composition trends (2–3-ring and 4–6-ring PAHs), we consider that historical energy usage in Northeast China can be divided into three stages: biomass fuel use dominated before 1920, biomass and fossil fuels co-existed from 1920 to 1980, and fossil fuels dominated after 1980. In addition, this study also demonstrates that the PAH concentrations (2–3-ring PAHs) in these two sediment cores can be used, to a certain extent, to identify anthropogenic fire events.

* Corresponding author. Key Laboratory of Coast and Island Development (Nanjing University), Ministry of Education, Nanjing 210093, China.
E-mail address: jhgao@nju.edu.cn (J. Gao).

https://doi.org/10.1016/j.chemosphere.2018.10.093
0045-6535/

1. Introduction

Polycyclic aromatic hydrocarbons (PAHs) are usually classified as environmental pollutants owing to their toxic, carcinogenic, mutagenic, and persistent characteristics. These compounds predominantly originate from anthropogenic activities, such as incomplete combustion of fossil fuels and biomass, vehicle emissions, etc. (Yunker et al., 2002; Han et al., 2015). In addition, natural processes, such as forest fires, can also contribute to high PAH concentrations over a regional scale (Vergnoux et al., 2011; Choi, 2014). Therefore, PAHs should not be classed solely as pollutants, but can also be used as geochemical markers of anthropogenic and natural activities (Liu et al., 2012; Denis et al., 2012; Ma et al., 2017). On the one hand, previous studies have demonstrated that vertical PAH concentration profiles in sediment cores can be used to reflect energy consumption and population density, and thus can reconstruct the economic development history of a region (Kannan et al., 2005; Guo et al., 2006; Lin et al., 2012; Bandowe et al., 2014). On the other hand, PAHs are byproducts of fire events, and so can be used as markers to reconstruct the history and intensity of local fires, and to aid paleofire research (Shen et al., 2011; Denis et al., 2012, 2017; Battistel et al., 2017).

Once PAHs are released into the environment, they will be present ubiquitously, including in the air, water, soil, sediment, and snow (Jiang et al., 2018; Wang et al., 2016a; b; Dudhagara et al., 2016; Parajulee et al., 2017; Wang et al., 2013). However, most PAHs are eventually deposited in marine sediments via two major pathways: riverine runoff and atmospheric precipitation. Therefore, marine sediments are considered important sinks of PAHs. Continental shelf mud deposits, which are usually elongated mud belts occurring along the coastline, represent a typical sedimentary system in coastal oceans, and have an abundant terrestrial sediment supply (Gao and Collins, 2014). Generally, mud deposits are predominantly composed of fine-grained sediments and have a relatively high deposition rate (Xu et al., 2012; Gao and Collins, 2014). These deposits are considered to be a significant sink for terrigenous materials, and consequently are an important sink for PAHs (Lin et al., 2013; Wang et al., 2017). Therefore, and because of their high resolution and continuous stratigraphic sequences, such sedimentary systems are generally considered ideal locations to study PAH histories (Guo et al., 2006, 2007; Liu et al., 2012). A number of mud deposits are located on the continental shelf of the Chinese marginal seas, including the mud belts of the Zhejiang-Fujian coast, Shandong Peninsula, Pearl River, and Liaodong Peninsula (Liu et al., 2007, 2014; Chen et al., 2013). Mud deposits near large-scale rivers, such as the Changjiang, Huanghe, and Pearl rivers, have attracted considerable attention over the past decade. However, the mud deposits along the southeastern coast of Liaodong Peninsula, which are controlled by small-scale rivers such as the Yalu, Zhuang, and Dayang rivers (Fig. 1), have received insufficient attention. The history of human activities in Northeastern China follows well-known variations that may be recorded in marine sediments. In addition, the Northeast is one of the three largest forest regions in China, and is very vulnerable to forest fires owing to its dry climate. Therefore, studies of PAHs in the mud deposits along the southeastern coast of Liaodong Peninsula are necessary, as they could aid understanding of the historical anthropogenic and natural activities in Northeast China.

Two sediment cores were collected from mud deposits along the southeastern coast of the Liaodong Peninsula. In this study, we attempted to reconstruct the histories of anthropogenic and natural activities in Northeast China, including economic development, population size, wars, and fire events, via the sedimentary PAH records of these cores.

2. Materials and methods

2.1. Regional setting

The study area, located along the southeastern coast of the Liaodong Peninsula, receives terrestrial matter from many rivers, including the Yalu River, providing a sediment discharge of 1.13×10^6 tons per year (Xu et al., 2018). In addition, the Dayang and Biliu rivers discharge considerable amounts of sediment (0.69×10^6 and 0.53×10^6 tons per year, respectively) into the study area (Xu et al., 2018). The circulation pattern is dominated by the Liaonan Coastal Current, which is predominantly formed by the Yalu River Diluted Water (Chen et al., 2013; Xu et al., 2018). Sediments discharged from the Yalu River are resuspended, transported southwestward over a long distance, and deposited along the southeastern coast of the Liaodong Peninsula to form mud deposits (Chen et al., 2013). The mud deposits along the southeastern coast of the Liaodong Peninsula were first noticed by Wang (2001), who discovered fine-grained deposits in a seismic profile. Chen et al. (2013) further explored its structures, provenance, and dynamic mechanisms. The mud deposits are up to 14 m thick and are distributed along the southeastern coast of the Liaodong Peninsula, 180–300 km from the Yalu River Estuary, and extend alongshore to Dalian Bay (Fig. 1), which has water depths of 20–40 m (Chen et al., 2013). Therefore, considerable amounts of information concerning anthropogenic and natural activities in the river basins may be recorded in this sedimentary system.

2.2. Sample collection

Sampling was carried out in March 2017 in the mud deposit along the Liaodong Peninsula. Two sediment cores, 02 (123°13.58′E, 39°34.46′N) and 04 (122°10.53′E, 39°02.10′N), were collected using a gravity corer, and their locations are shown in Fig. 1. The length of the sediment cores obtained at the 02 and 04 sites were 300 cm and 330 cm, respectively. The upper 100 cm of the two cores were sectioned at approximately 2 cm intervals and placed in aluminum foil cleaned with n-hexane. Each section was then freeze-dried, homogenized, and stored at −20 °C prior to analysis.

2.3. Grain-size analysis

All samples were dispersed in sodium metaphosphate for 24 h, and then dispersed and homogenized using an ultrasonicator for 30 s to ensure the sediment was fully dispersed. The grain-size composition of the samples was measured using a laser diffraction particle size analyzer (Mastersizer 2000, Malven Instruments Ltd., UK) with a measuring error of less than 3%. Grain-size parameters, including the mean, sorting coefficient, skewness, and kurtosis were calculated using the Mcmanus (1988) formulae.

2.4. ^{210}Pb analysis and dating

^{210}Pb analyses were performed on the two sediment cores to determine the sediment ages. 2–3 g of sediment powder was spiked with a known volume of ^{209}Po and digested in concentrated HF, HNO_3, and HCl. Then, ^{209}Po and ^{210}Po were plated onto nickel planchets and counted by alpha spectroscopy to determine the total ^{210}Pb activity. ^{226}Ra-supported activity was assumed to equal a low uniform value below the radioactive decay section of the sediment cores (Palinkas and Nittrouer, 2007; Szczuciński et al., 2009), and the unsupported (excess) ^{210}Pb ($^{210}Pb_{ex}$) activity was extracted from the total activity. The deposition rate was determined from the logarithmic regression profile of $^{210}Pb_{ex}$ versus

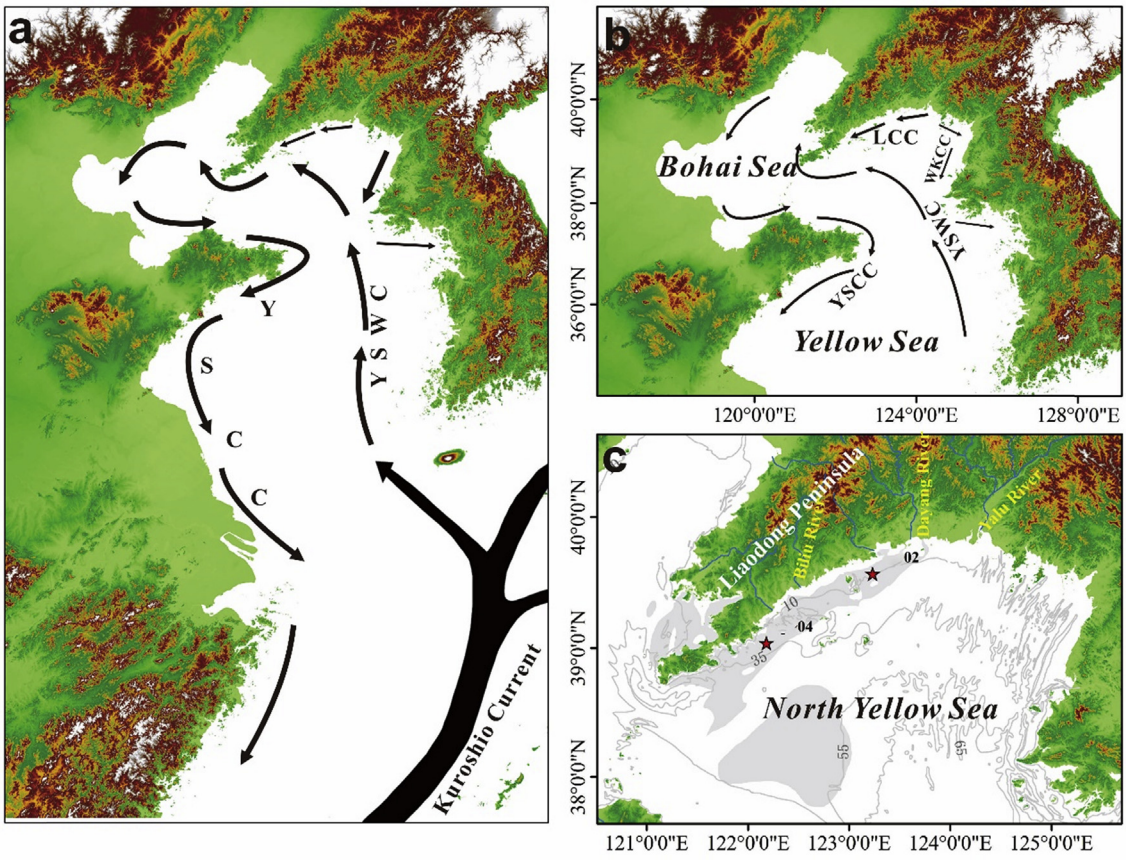

Fig. 1. Study area and location of sampling sites. YSWC: Yellow Sea Warm Current; YSCC: Yellow Sea Coastal Current; LCC: Liaonan Coastal Current; WKCC: West Korea Coastal Current.

depth using the constant initial concentration (CIC) model (Robbins and Edgington, 1975; Mckee et al., 1983).

2.5. PAH extraction and analysis

PAH extraction followed the method reported by Wang et al. (2016a). Approximately 10 g of sediment were freeze-dried, ground, and spiked with a mixture of recovery standards consisting of five deuterated PAHs (acenaphthene-d_{10}, phenanthrene-d_{10}, chrysene-d_{12}, perylene-d_{12}, and naphthalene-d_8). The samples were Soxhlet extracted using 100 mL of n-hexane/acetone (1:1 v/v) over 24 h, and 2 g activated copper was added to remove sulfur. The extracted solution was concentrated to approximately 1 mL, and fractionated using a chromatography column (25 cm × 1 cm, internal diameter) with 5 g silica gel and 2 cm anhydrous sodium sulfate. The concentrated solution was eluted with 50 mL n-hexane/dichloromethane (3:2 v/v), and then concentrated, solvent-exchanged with n-hexane, and finally concentrated to 1 mL.

Denis et al. (2012) demonstrated that high-performance liquid chromatography with a fluorescence detector (HPLC-FLD) has a higher sensitivity than gas chromatography mass spectrometry for detecting PAHs. Therefore, HPLC-FLD was selected to analyze PAHs in this study, using the method described in Denis et al. (2012) and the National Environmental Protection Standards of China (Ministry of environmental protection of the People's Republic of China, 2016). The samples were analyzed using an Agilent 1200 series chromatograph with a binary pump interfaced to a diode array detector (DAD) and fluorescence detector. A 16-PAH standard mixture solution (Supelco, Bellefonte, PA, USA) was obtained to develop the DAD method to assess the separation and elution order of PAHs. This method was then developed on the FLD to optimize the signal for each PAH compound while maintaining a suitable chromatogram. Separations were performed with a 25 cm × 4.6 mm (length × internal diameter), 5.0-μm particle, Supelcosil LC-PAH obtained from Supelco. The temperature of the HPLC column was kept constant at 35 °C to obtain reproducible PAH retention times. This reproducibility is of paramount importance when using a defined wavelength program, which allows sensitivity optimization for each PAH. Acetonitrile (ACN) and water were used as mobile phases. The gradient was managed as follows: a 60:40 ACN:H_2O combination was used for 8 min, followed by a change to 100:0 ACN:H_2O over 18 min, which was then held constant for 28 min, followed by a change to 60:40 ACN:H_2O over 28.5 min, which was then held constant for 35 min. The injection volume was set to 10 μL via an LC flow rate of 1 mL/min. Detection was performed at selected excitation and emission wavelengths (Table 1). The following PAHs were analyzed: naphthalene (Nap), acenaphthene (Ace), fluorene (Flu), phenanthrene (Phe), anthracene (Ant), fluoranthene (Flo), pyrene (Pyr), benz[a]anthracene (BaA), chrysene (Chr), benzo[b]fluoranthene (BbF), benzo[k]fluoranthene (BkF), benzo[a]pyrene (BaP), dibenz[ah]anthracene (DahA), indeno[123cd]pyrene (IcdP), and benzo[g,h,i]perylene (BghiP).

A procedural blank and spiked samples were analyzed with every 12 samples. Duplicates were run every 12 samples, and samples were reanalyzed if differences exceeded 15%. PAHs were quantified using the external standard method. Calibration curves were drawn based on sets of five standard concentrations: 10 ng/L,

Table 1
Wavelength detection program for quantification of PAHs.

Peak order	PAHs	Recommended $\lambda_{ex}/\lambda_{em}$	Optimum $\lambda_{ex}/\lambda_{em}$
1	Nap	280/324	280/334
2	Ace	280/324	268/308
3	Flu	280/324	280/324
4	Phe	254/350	292/366
5	Ant	254/400	253/402
6	Flo	290/460	360/460
7	Pyr	336/376	336/376
8	BaA	275/385	288/390
9	Chr	275/385	268/383
10	BbF	305/430	300/436
11	BkF	305/430	308/414
12	BaP	305/430	296/408
13	DahA	305/430	297/398
14	BghiP	305/430	300/410
15	IcdP	305/500	302/506

50 ng/L, 100 ng/L, 250 ng/L, and 500 ng/L. The standard curve was checked daily using the reference standard to ensure satisfactory linear regression coefficients ($R^2 > 0.999$) for all tested PAHs. Average PAH recoveries based on spiked samples ranged from 74.0% to 92.5%. Detection limits were calculated as being three times the standard deviation of the blank concentrations, which were between 0.1 ng/g and 0.5 ng/g for all analytes.

3. Results and discussion

3.1. ^{210}Pb dating and sedimentary features

The total ^{210}Pb activities of cores 02 and 04 are shown in Fig. 2, which displays apparent decay and the background region. Core 02 exhibited normal decay of ^{210}Pb activity in the upper 39 cm, and a background region below 39 cm. A similar trend was observed in core 04, which showed normal decay in the upper 29 cm, and a background region below 29 cm. The excess ^{210}Pb ($^{210}Pb_{ex}$) activities of cores 02 and 04 are displayed in Fig. 2, which shows an obvious exponential decay trend. The constant initial concentration model was used to calculate deposition rates in this study, and the results give deposition rates of 0.31 cm/a and 0.23 cm/a for cores 02 and 04, respectively.

The results of grain-size analyses show that the sediments in cores 02 and 04 were dominated by silt (Fig. 3a). The average percentages of silt, clay, and sand in core 02 were 68%, 27%, and 5%, respectively. The content of fine-grained sediments, which consisted of silt and clay and are generally termed “mud deposits,” in the down-core was nearly constant (Fig. 3a), indicating a stable sedimentary environment in this region. Core 02 was dominated by silt with an average grain-size of 7.03 ± 0.48 Φ. The vertical trend in the sediment grain-sizes in core 04 shows clear differences when compared with core 02 (Fig. 3b). Although core 04 was dominated by mud deposits, it also had a relatively high sand content. The average contents of silt, clay, and sand in core 04 were 64%, 16%, and 20%, respectively. The vertical trend in the sediment grain-size in core 04 can be divided into three stages (Fig. 3b), including a coarser trend from the bottom up to the surface. However, the sediment grain-sizes show consistency within each stage, which indicates a stable sedimentary environment in this region.

According to the vertical distribution trends of ^{210}Pb and sediment grain-sizes, we considered that these two sediment cores were ideal materials to study anthropogenic and natural activities in the river basins. In this study, we attempted to reconstruct the economic development history of northeast China via the sedimentary PAH records, and to explore whether this proxy could be used to provide information on wars and even fire events.

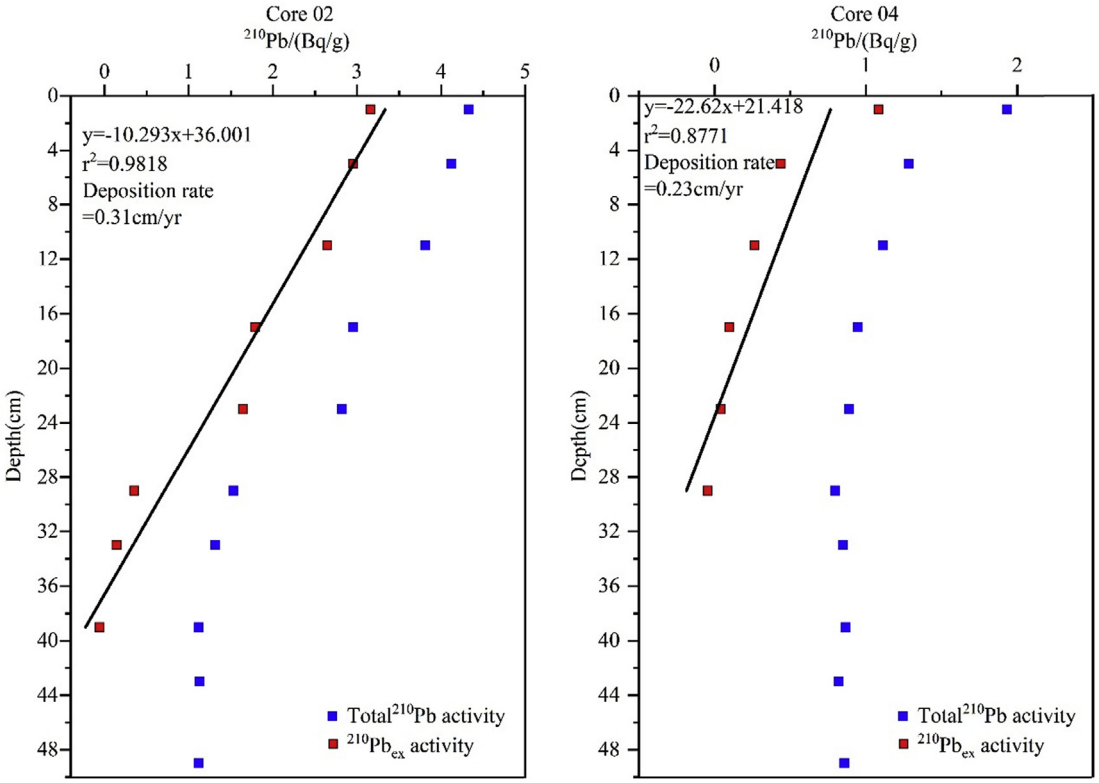

Fig. 2. Sediment records of ^{210}Pb and recent accumulation rates for the sediment cores.

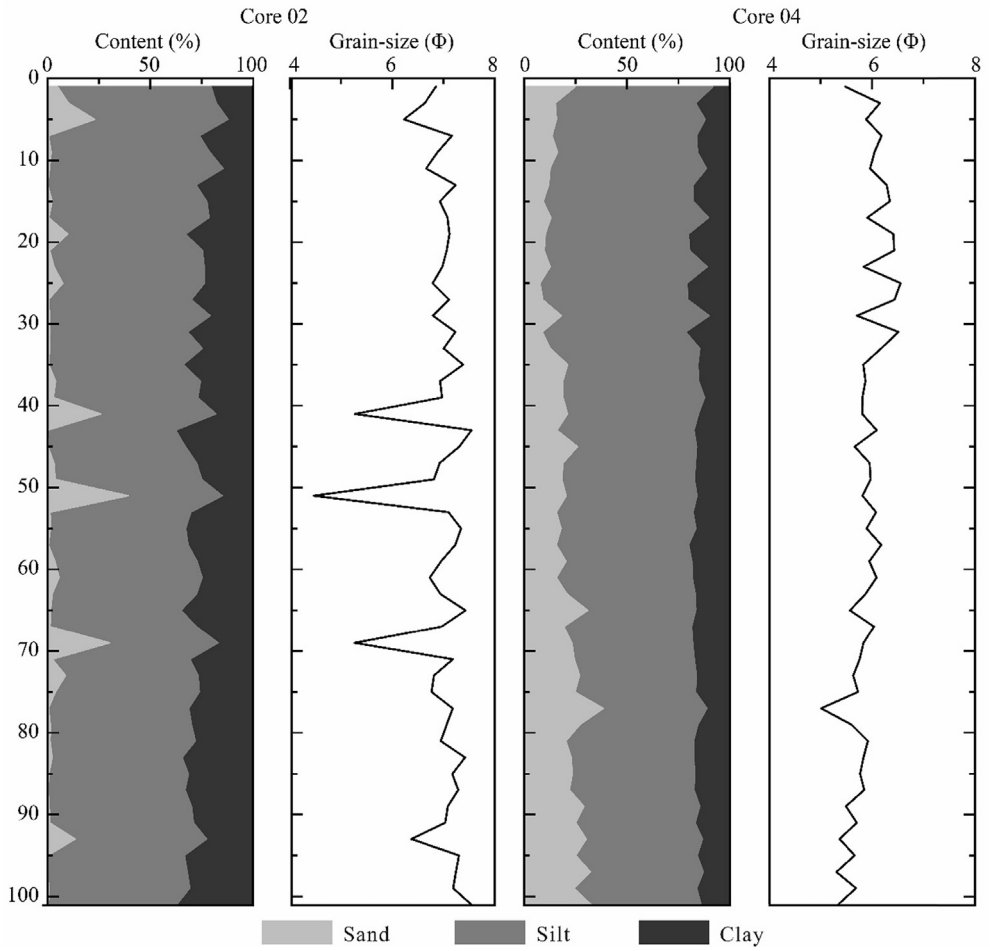

Fig. 3. Grain-size variations in sediment cores 02 and 04.

3.2. Historical variations of the 16 PAH concentrations

The vertical distributions of the 16 PAH concentrations (∑PAHs) in cores 02 and 04 are displayed in Fig. 4. The ∑PAH levels in core 02 ranged from 3.9 to 211.5 ng/g, with an average concentration of 50.5 ng/g. The ∑PAH levels in core 04 ranged from 1.8 to 234.6 ng/g, with an average concentration of 52.1 ng/g. There were obvious differences in the vertical distribution trends of ∑PAHs between core 02 and 04, especially in regard to the period that PAHs began to increase (Fig. 4). The vertical distribution of ∑PAHs in core 02 showed a clear increasing trend after 1890 but, in core 04, this turning point occurred in the 1820s (Fig. 4). Previous studies have demonstrated that sedimentary records of PAHs can be used to reconstruct socio-economic history, and they generally show an increasing trend in China after the Opium Wars (1840) (Fig. 5) (Guo et al., 2006, 2007; Liu et al., 2012; Ma et al., 2017) because the Westernization Movement (1860s), which forced the initiation of industrialization in China, occurred after this period. However, this typical phenomenon did not occur in our study, and our results display completely different increasing trends (Fig. 4). To better understand their difference, we collected sediment cores from tidal flats, coastal oceans, and inland lakes throughout the nation, which are displayed in Fig. S1. The vertical distribution of ∑PAHs in core 02 showed stable low PAH concentrations before 1890, which may reflect an autarkic agricultural civilization (Guo et al., 2006; Ma et al., 2017). In core 04, ∑PAH concentrations began to increase after 1820; this variation began earlier than the Westernization Movement in the 1860s, and earlier than that in core 02. Therefore, the vertical distribution patterns of PAHs in our study area appear not to have been strongly influenced by the Westernization Movement. Although there was a clear increasing trend in ∑PAH levels in core 04 after 1840 (the First Opium War), this signal cannot reflect the Westernization Movement, due to the fact that a prohibition policy forbidding population migration and industrial development was implemented in Northeast China by the Qing Government in 1668. Under the influence of this prohibition, Northeast China remained in a relatively primitive state for a long time. After the prohibition was broken, some population migration occurred, thereby accelerating agricultural development in Northeast China (Fig. 5). Therefore, government intervention could have been the primary influence upon the vertical distribution trend of PAHs in the Northeast China in the 1800s. Although the vertical distribution ∑PAH trends in cores 02 and 04 do not reflect national trends, they do reflect the local economic development of Northeast China. We also explored why the PAH increases in cores 02 and 04 began at different times, and found an explanation in their sampling locations (Fig. 1c). Core 04 was located nearby Dalian City, a region that saw relatively high levels of development in the early 1820s. However, core 02 was located far from the developed regions, and was probably only influenced by human activities in the middle and late 1800s after the large population influx to Northeast China (Fig. 5). Therefore, the intensity of human activity could be a dominant factor that determined the vertical distribution patterns for PAHs in these two cores.

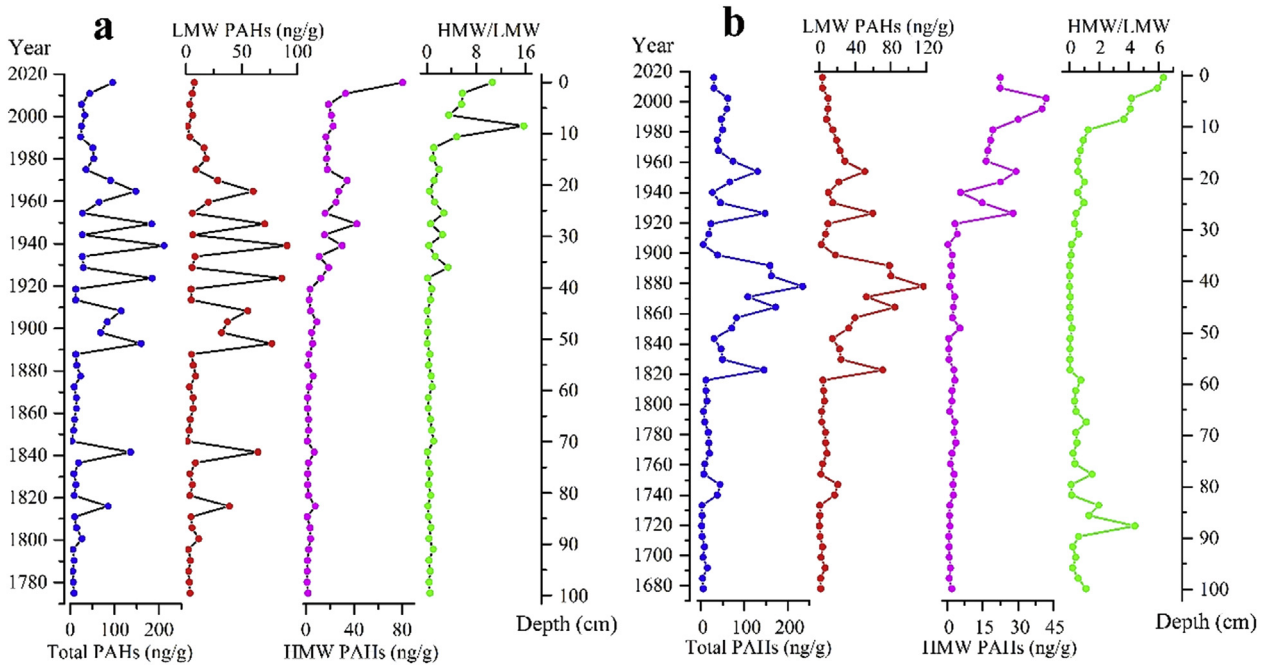

Fig. 4. Vertical distribution trends of ∑PAHs, LMW PAHs, HMW PAHs, and HMW/LMW in (a) core 02 and (b) core 04.

From the beginning of the 1880s in core 02, and the 1820s in core 04, ∑PAH levels displayed increasing trends with significant fluctuations, which could reflect the close relationship between economic and social stability determined by factors such as migration and wars. The prohibition of the Qing Government gradually eased in the early 1800s, resulting in the first ∑PAH peak occurring in 1820 (Fig. 4). In this period, some people migrated into Northeast China, resulting in the release of large amounts of PAHs into the environment over this period. In addition, the vertical distribution trends of the PAH levels for this period are consistent with the population migration which began in the early 1800s (Fig. 5). The increase in PAH levels became more rapid in core 04 between 1840 and the 1880s, culminating in a ∑PAH peak at 1880, which also occurred at this period in core 02. The vertical distribution patterns of PAHs in core 02 and 04 displayed increasing trends with significant fluctuations after 1900 (Fig. 4), which could be due to the fact that Northeast China entered a period of social turbulence with continuous wars after 1900. At the same time, the population size in Northeast China dramatically increased (Fig. 5). Relatively low ∑PAH levels occurred in core 02 in 1900, 1920, 1930, and in the early 1940s, which could reflect wars, such as the Russo-Japanese War (1904–1905), the Mukden Incident (1931), the Anti-Japanese War (1937–1945), and the Liberation War (1945–1949). In addition, rapid increasing ∑PAH trends can be observed after the wars, suggesting typical post-war resumption of production. Similar low ∑PAH levels can also be seen in core 04 in 1900, 1920, 1930, and 1940, but the phenomenon is not as obvious as in core 02 because of the relatively low time-resolution of core 04. Therefore, from the beginning of the 1900s to the late 1940s, the observed ∑PAH fluctuations correspond to known social turbulence in Northeast China.

The vertical distribution pattern of PAHs in core 02 can be used to reflect socio-economic development after the founding of the People's Republic of China (1949) due to its relatively high temporal resolution. PAHs began to increase after 1953 and peaked in the mid-1960s, before beginning to decrease and forming a dip in the mid-1970s (Fig. 4a). These variation trends are more consistent with the socio-economic development of this period. After 1949, production quickly resumed and the "Five Year Plan" was implemented (1953), which caused rapid socio-economic development. However, the Cultural Revolution occurred during 1966–1976, which resulted in the closure or reduced production of many manufacturing plants during this period (Guo et al., 2006). After the Cultural Revolution, the PAHs began to increase in core 02 due to the "Reform and Open" Policy implemented in 1978, which resulted in an accelerated rate of economic development. At the same time, the gross domestic product and energy consumption in Northeast China drastically increased, which is also reflected in the PAH sedimentary record of core 02 (Fig. 5).

3.3. Vertical trends for high molecular weight (HMW) and low molecular weight (LMW) PAHs

The concentrations of LMW PAHs (2–3-ring PAHs) and HMW PAHs (4–6-ring PAHs) are also displayed in Fig. 4. Previous studies have demonstrated that LMW PAHs predominantly originate from low and moderate temperature burning processes, such as biomass burning, whereas HMW PAHs are predominantly formed by high temperature burning processes, such as fossil fuel combustion. In addition, the ratio of individual PAHs, such as Flu/(Flu + Pyr), IcdP/(IcdP + BghiP), and Ant/(Ant + Phe), were also used to identify PAH sources. However, these indicators could not be used in this study due to low PAH concentrations, some of which were lower than the detection limit, which resulted in these indicators losing their efficacy. Therefore, we used HMW PAHs and LMW PAHs to replace the isomer ratio method to identify PAH sources and energy usage trends (Guo et al., 2006; Zhang et al., 2013; Ma et al., 2017). As expected, vertical distributions of LMW PAHs in cores 02 and 04 show similar variation trends to ∑PAH levels during 1920–1980. Therefore, the vertical distributions of ∑PAH levels in cores 02 and 04 can be divided into three stages: before 1920, 1920–1980, and after 1980. Before 1920, the concentrations of HMW PAHs were very low in cores 02 and 04, and the ∑PAH levels predominantly consisted of LMW PAHs, which suggests an agricultural society

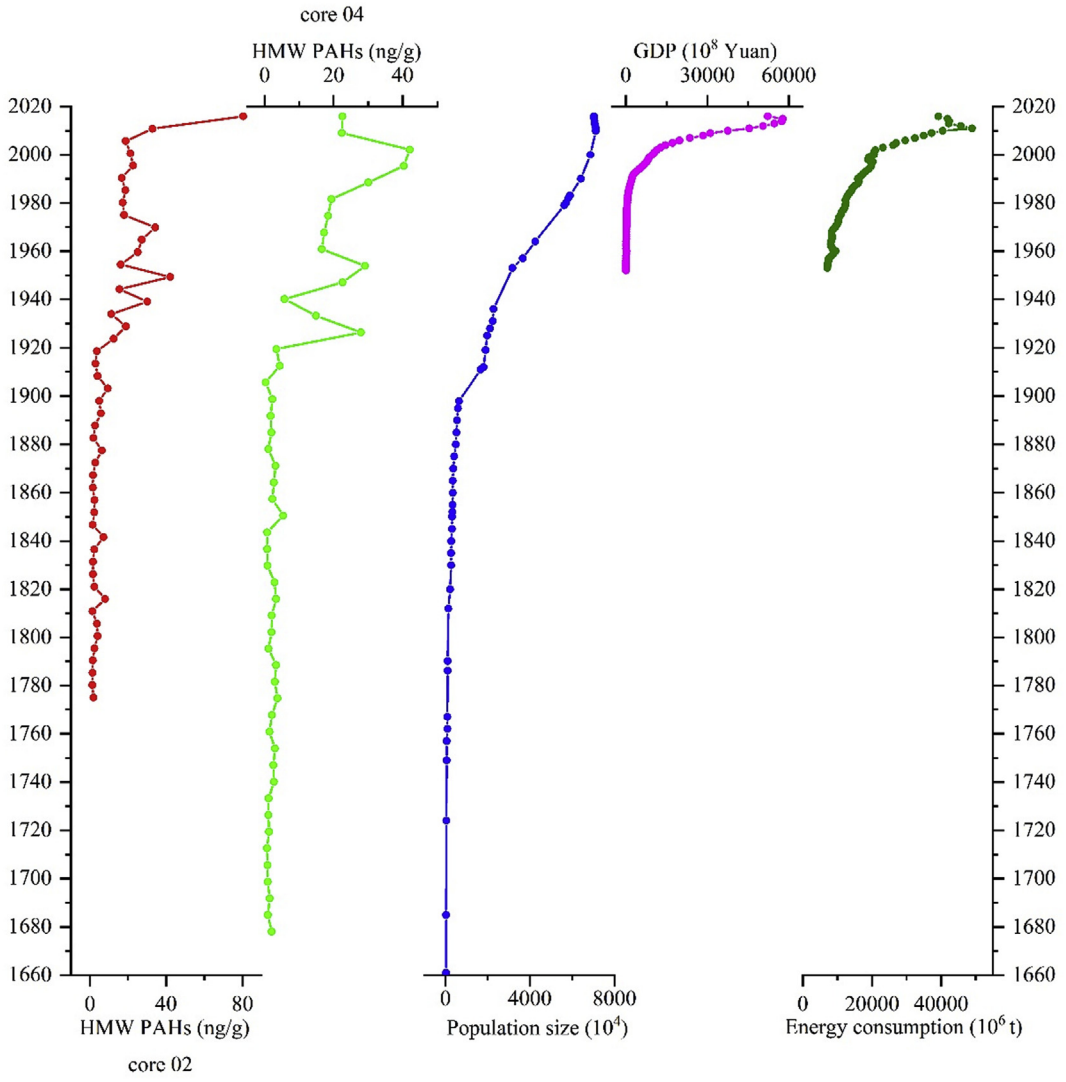

Fig. 5. Vertical distributions of HMW PAH concentrations in cores 02 and 04 compared with population and total energy consumption trends.

dominated by biomass fuels. This situation is consistent with the socio-economic development of Northeast China governed by the prohibition of the Qing Government. During 1920–1980, although the vertical ∑PAH trends were consistent with those of the LMW PAHs, the concentrations of HMW PAHs began to increase, which changed the ∑PAH composition. Early in this period (1920–1949), Northeast China entered a period of social turbulence with continuous wars, and large amounts of fossil fuels, such as coal and oil, were consumed. Therefore, the ratios of HMW/LMW in core 02 and 04 displayed a fluctuating upward trend. During 1949–1980, the ∑PAH compositions were a combination of LMW and HMW PAHs, and the proportion of HMW PAHs gradually increased. After 1980, HMW PAHs dominated cores 02 and 04, and the concentrations of LMW PAHs show a marked decrease. However, the HMW PAHs in core 04 displayed an obvious decreasing trend in the surface layer (down to 6 cm), which was different from the trend in core 02 (Fig. 4). This phenomenon was unexpected, and we carefully considered the factors that may have led to this decreasing trend; we determined that human disturbance due to intensive farming activities in this region could have been the primary factor that influenced the vertical distribution trend of PAHs in core 04. Additionally, the ratio of HMW/LMW showed an increased trend, which suggested that this indicator can also be used to identify PAH sources. In this period, the Northeast was the most important heavy industry base in China, with developed energy, steel, and machine manufacturing industries. Data on the energy consumption, population, and GDP value in Northeast China was collected, and displayed an increasing trend after 1980 (Fig. 5), which had a good correspondence to the vertical distribution trend of HMW/LMW. Therefore, the energy source trends of Northeast China can be divided into three stages: biomass fuels dominated before 1920, biomass and fossil fuels co-existed during 1920–1980, and fossil fuels dominated after 1980.

3.4. Detection of fires events

Previous studies have demonstrated that LMW PAHs predominantly originate from low and moderate temperature combustion processes such as biomass burning, and so can be used to identify historical fire events (Denis et al., 2012; Bandowe et al., 2014). Therefore, we also attempted to detect fire events in this study using the vertical distribution trends of LMW PAHs in cores 02 and 04. Before 1900, some peaks in the LMW PAH concentrations were detected; for example, peaks in 1820 and 1890 were detected in

both cores. In this period, large amounts of refugees moved into Northeast China, and a large number of grassland and forest areas were burnt down to provide land. In addition, another peak in the LMW PAH levels was also found in core 02 in 1840. Before 1900, there was little industrial activity in Northeast China, and ∑PAH levels were dominated by LMW PAHs (Fig. 4). However, after 1900, the concentrations of HMW PAHs in the sediment cores began to increase and overwhelmed LMW PAH concentrations. Overall, the concentrations of LMW PAHs in these two sediment cores can be used to identify anthropogenic fire events to a certain extent.

4. Conclusions

In this study, historical trends of ∑PAHs, LMW PAHs, and HMW PAHs were investigated in dated sediment cores from mud deposits along the southeastern coast of the Liaodong Peninsula to reconstruct the sedimentary records of PAHs and investigate their response to anthropogenic and natural activities. The results of ^{210}Pb dating and sediment grain-size analyses in cores 02 and 04 show a relatively stable sedimentary environment in the study area, and the sedimentary sequences are continuous. Therefore, these two sediment cores provided ideal material to study the anthropogenic and natural activity histories in the river basins. The ∑PAH levels, mainly consisting of 2–3-ring PAHs, significantly increased from 1820 to 1890. This increase was due to the growing population and developing agriculture caused by the end of the Qing Government's prohibition. From the beginning of the 1900s, ∑PAH levels displayed an increasing trend with significant fluctuations, which could reflect the close relationship between economic and social stability, especially as observed during wars. Simultaneously, the concentrations of HMW PAHs gradually began to increase. After the founding of the People's Republic of China (1949), the ∑PAH and HMW PAH levels showed good degrees of correspondence with socio-economic development. The different vertical trends of LMW PAHs and HMW PAHs clearly reflect the transition of energy usage from biomass burning to fossil fuel combustion. Therefore, the energy usage trends of Northeast China can be divided into three stages: biomass fuels dominated before 1920, biomass and fossil fuels co-existed during 1920–1980, and fossil fuels dominated after 1980. In addition, sedimentary records of LMW PAHs in these two sediment cores can be used to identify anthropogenic fire events, with some limitations.

Acknowledgement

The study was supported by the Natural Science Foundation of China (grants 41576043, 41625021, and 41476052). The data for this paper are available by contacting the corresponding author.

Appendix A. Supplementary data

Supplementary data to this article can be found online at https://doi.org/10.1016/j.chemosphere.2018.10.093.

References

Bandowe, B.A.M., Srinivasan, P., Seelge, M., Sirocko, F., Wilcke, W., 2014. A 2600-year record of past polycyclic aromatic hydrocarbons (PAHs) deposition at Holzmaar (Eifel, Germany). Palaeogeogr. Palaeoclimatol. Palaeoecol. 401 (5), 111–121.

Battistel, D., Argiriadis, E., Kehrwald, N., Spigariol, M., Russell, J.M., Barbante, C., 2017. Fire and human record at lake Victoria, east Africa, during the early iron age: did humans or climate cause massive ecosystem changes? Holocene 27 (7), 997–1007.

Chen, X., Li, T., Zhang, X., Li, R., 2013. A Holocene Yalu River-derived fine-grained deposit in the southeast coastal area of the Liaodong Peninsula. Chin. J. Oceanol. Limnol. 31 (3), 636–647.

Choi, S.D., 2014. Time trends in the levels and patterns of polycyclic aromatic hydrocarbons (PAHs) in pine bark, litter, and soil after a forest fire. Sci. Total Environ. 470–471 (2), 1441–1449.

Denis, E.H., Toney, J.L., Tarozo, R., Anderson, R.S., Roach, L.D., Huang, Y., 2012. Polycyclic aromatic hydrocarbons (PAHs) in lake sediments record historic fire events: validation using HPLC-fluorescence detection. Org. Geochem. 45 (2), 7–17.

Denis, E.H., Pedentchouk, N., Schouten, S., Pagani, M., Freeman, K.H., 2017. Fire and ecosystem change in the Arctic across the paleocene-eocene thermal maximum. Earth Planet Sci. Lett. 467, 149–156.

Dudhagara, D.R., Rajpara, R.K., Bhatt, J.K., Gosai, H.B., Sachaniya, B.K., Dave, B.P., 2016. Distribution, sources and ecological risk assessment of PAHs in historically contaminated surface sediments at Bhavnagar coast, Gujarat, India. Environ. Pollut. 213, 338–346.

Gao, S., Collins, M.B., 2014. Holocene sedimentary systems on continental shelves. Mar. Geol. 352 (3), 268–294.

Guo, Z., Lin, T., Zhang, G., Yang, Z., Fan, M., 2006. High-resolution depositional records of polycyclic aromatic hydrocarbons in the central continental shelf mud of the East China Sea. Environ. Sci. Technol. 40 (17), 5304–5311.

Guo, Z., Lin, T., Zhang, G., Zheng, M., Zhang, Z., Hao, Y., et al., 2007. The sedimentary fluxes of polycyclic aromatic hydrocarbons in the Yangtze River Estuary coastal sea for the past century. Sci. Total Environ. 386 (1), 33–41.

Han, Y.M., Wei, C., Bandowe, B.A.M., Wilcke, W., Cao, J.J., Xu, B.Q., et al., 2015. Elemental carbon and polycyclic aromatic compounds in a 150-year sediment core from lake Qinghai, Tibetan Plateau, China: influence of regional and local sources and transport pathways. Environ. Sci. Technol. 49 (7), 4176–4183.

Jiang, Y., Lin, T., Wu, Z., Li, Y., Li, Z., Guo, Z., et al., 2018. Seasonal atmospheric deposition and air–sea gas exchange of polycyclic aromatic hydrocarbons over the Yangtze River Estuary, East China Sea: implications for source–sink processes. Atmos. Environ. 178, 31–40.

Kannan, K., Johnson, R., Yohn, S., Long, R., 2005. Spatial and temporal distribution of polycyclic aromatic hydrocarbons in sediments from Michigan inland lakes. Environ. Sci. Technol. 39 (13), 4700–4706.

Lin, T., Hu, L., Guo, Z., Zhang, G., Yang, Z., 2013. Deposition fluxes and fate of polycyclic aromatic hydrocarbons in the Yangtze River estuarine-inner shelf in the East China Sea. Global Biogeochem. Cycles 27 (1), 77–87.

Lin, T., Qin, Y., Zheng, B., Li, Y., Lei, Z., Guo, Z., 2012. Sedimentary record of polycyclic aromatic hydrocarbons in a reservoir in Northeast China. Environ. Pollut. 163 (4), 256–260.

Liu, L.Y., Wang, J.Z., Wei, G.L., Guan, Y.F., Wong, C.S., Zeng, E.Y., 2012. Sediment records of polycyclic aromatic hydrocarbons (PAHs) in the continental shelf of China: implications for evolving anthropogenic impacts. Environ. Sci. Technol. 46 (12), 6497–6504.

Liu, J.P., Xu, K.H., Li, A.E.A., Milliman, J.D., Velozzi, D.M., Xiao, S.B., Yang, Z.S., 2007. Flux and fate of Yangtze river sediment delivered to the east China sea. Geomorphology 85 (3), 208–224.

Liu, Y., Gao, S., Wang, Y.P., Yang, Y., Long, J., Zhang, Y., et al., 2014. Distal mud deposits associated with the pearl river over the northwestern continental shelf of the South China Sea. Mar. Geol. 347 (1), 43–57.

Ma, C., Lin, T., Ye, S., Ding, X., Li, Y., Guo, Z., 2017. Sediment record of polycyclic aromatic hydrocarbons in the Liaohe River delta wetland, Northeast China: implications for regional population migration and economic development. Environ. Pollut. 222, 146–152.

Mcmanus, J., 1988. Grain size determination and interpretation. Tech. Sedimentol. 408, 112–116.

Mckee, B.A., Nittrouer, C.A., Demaster, D.J., 1983. Concepts of sediment deposition and accumulation applied to the continental shelf near the mouth of the Yangtze river. Geology 87 (2-3), 1354–1360.

Ministry of environmental protection of the People's Republic of China, 2016. Soil and Sediment—Determination of Polycyclic Aromatic Hydrocarbons-High Performance Liquid Chromatography. HJ 784-2016.

Parajulee, A., Lei, Y.D., Kananathalingam, A., Mclagan, D.S., Cpj, M., Wania, F., 2017. The transport of polycyclic aromatic hydrocarbons during rainfall and snowmelt in contrasting landscapes. Water Res. 124, 407–414.

Palinkas, C.M., Nittrouer, C.A., 2007. Modern sediment accumulation on the Po shelf, Adriatic Sea. Continent. Shelf Res. 27 (3), 489–505.

Robbins, J.A., Edgington, D.N., 1975. Determination of recent sedimentation rates in lake Michigan using pb-210 and cs-137. Geochem. Cosmochim. Acta 39 (3), 285–304.

Shen, W., Sun, Y., Lin, Y., Liu, D., Chai, P., 2011. Evidence for wildfire in the Meishan section and implications for Permian–Triassic events. Geochem. Cosmochim. Acta 75 (7), 1992–2006.

Szczuciński, W., Zajączkowski, M., Scholten, J., 2009. Sediment accumulation rates in subpolar fjords – impact of post-little ice age glaciers retreat, Billefjorden, Svalbard. Estuar. Coast Shelf Sci. 85 (3), 345–356.

Vergnoux, A., Malleret, L., Asia, L., Doumenq, P., Theraulaz, F., 2011. Impact of forest fires on PAH level and distribution in soils. Environ. Res. 111 (2), 193–198.

Wang, C., Zou, X., Gao, J., Zhao, Y., Yu, W., Li, Y., et al., 2016a. Pollution status of polycyclic aromatic hydrocarbons in surface sediments from the Yangtze River Estuary and its adjacent coastal zone. Chemosphere 162, 80–90.

Wang, C., Zou, X., Zhao, Y., Li, B., Song, Q., Li, Y., et al., 2016b. Distribution, sources, and ecological risk assessment of polycyclic aromatic hydrocarbons in the water and suspended sediments from the middle and lower reaches of the Yangtze River, China. Environ. Sci. Pollut. R. 23 (17), 1–13.

Wang, C., Zou, X., Zhao, Y., Li, Y., Song, Q., Wang, T., et al., 2017. Distribution pattern and mass budget of sedimentary polycyclic aromatic hydrocarbons in shelf

areas of the Eastern China Marginal Seas. J. Geophys. Res. Ocean 122 (6), 4990–5004.
Wang, X., Miao, Y., Zhang, Y., Li, Y., Wu, M., Yu, G., 2013. Polycyclic aromatic hydrocarbons (PAHs) in urban soils of the megacity Shanghai: occurrence, source apportionment and potential human health risk. Sci. Total Environ. 447 (1), 80–89.
Wang, G., 2001. Sedimentary Characteristics and Mechanism of Mud Deposit in the Northern Yellow Sea. Ph. D. Thesis. Institute of Oceanology, Chinese Academy of Sciences, Qingdao, China (in Chinese with English abstract).
Xu, K., Li, A., Liu, J.P., Milliman, J.D., Yang, Z., Liu, C.S., et al., 2012. Provenance, structure, and formation of the mud wedge along inner continental shelf of the East China Sea: a synthesis of the Yangtze dispersal system. Mar. Geol. 291–294 (4), 176–191.
Xu, Y., Pan, S., Gao, J., Hou, X., Ma, Y., Hao, Y., 2018. Sedimentary record of plutonium in the north yellow sea and the response to catchment environmental changes of inflow rivers. Chemosphere 207, 130–138.
Yunker, M.B., Macdonald, R.W., Vingarzan, R., Mitchell, R.H., Goyette, D., Sylvestre, S., 2002. PAHs in the Fraser river basin: a critical appraisal of PAH ratios as indicators of PAH source and composition. Org. Geochem. 33 (4), 489–515.
Zhang, R., Zhang, F., Zhang, T.C., 2013. Sedimentary records of PAHs in a sediment core from tidal flat of Haizhou Bay, China. Sci. Total Environ. S450–451 (450–451C), 280–288.